Available online at www.sciencedirect.com
SCIENCE DIRECT®
Chemical Physics Letters 376 (2003) 588–594
CHEMICAL PHYSICS LETTERS
www.elsevier.com/locate/cplett

# Electronic spectroscopy of predissociative states of platinum oxide cation

Christopher J. Thompson, Kay L. Stringer, Melanie McWilliams, Ricardo B. Metz *

*Department of Chemistry, University of Massachusetts-Amherst, Lederle GRC, Amherst, MA 01003, USA*

Received 29 April 2003; in final form 16 June 2003
Published online: 9 July 2003

**Abstract**

The photodissociation spectrum of jet-cooled $PtO^+$ is reported over the range of 25 000 to 30 000 $cm^{-1}$. Excited state vibrational progressions are identified for $^4\Pi_{-1/2} \leftarrow {}^4\Sigma_{3/2}$ and $^4\Pi_{5/2} \leftarrow {}^4\Sigma_{3/2}$ transitions with several vibrational peaks rotationally resolved. Additional peaks not assigned to a vibrational series also exhibit rotational structure. Transitions arising from the $^4\Sigma_{3/2}$ ground state show a spectroscopic onset of 25 520 $cm^{-1}$, giving an upper limit to the bond strength of $D_0(Pt^+–O) \leqslant 305$ kJ $mol^{-1}$. A hot band is observed at 25 317 $cm^{-1}$ and rotational analysis predicts it as arising from a low-lying $\Omega = 7/2$ state, probably $^4\Delta_{7/2}$.


## 1. Introduction

As one of the most abundant, simple and inexpensive hydrocarbons, methane is of considerable economic value. However, being a permanent gas, methane is expensive to transport and is not easily converted to more useable products such as methanol or gasoline. It is of both technological and fundamental interest to find a direct way to convert methane into methanol [1–3]. Transition metal oxides, $MO^+$, have been shown to efficiently and directly convert methane to methanol under thermal conditions in the gas phase [4,5]. Specifically, the reaction of $PtO^+$ with methane occurs at the collision rate and produces methanol with 25% selectivity [6]

$$PtO^+ + CH_4 \rightarrow Pt^+ + CH_3OH \quad (1)$$

This simple reaction serves as a key step in the gas-phase catalytic conversion of methane to methanol by bare $Pt^+$ [7]. The cycle begins with methane reacting with $Pt^+$ to form the $PtCH_2^+$ intermediate. Using $O_2$ as the oxidant, the following reactions occur:

$$PtCH_2^+ + O_2 \rightarrow PtO^+ + CH_2O\ (30\%) \quad (2)$$

$$PtCH_2^+ + O_2 \rightarrow Pt^+ + [C,H_2,O_2]\ (70\%) \quad (3)$$

* Corresponding author. Fax: +1-413-545-4490.
*E-mail address:* rbmetz@chemistry.umass.edu (R.B. Metz).

0009-2614/$ - see front matter © 2003 Elsevier B.V. All rights reserved.
doi:10.1016/S0009-2614(03)01046-7

The catalytic cycle then uses reaction (1) to produce methanol and regenerate $Pt^+$, continuing the cycle.

Gas-phase studies of $MO^+$ are useful because these catalytic species are examined without interference of solvent or other ligands and thus serve as good model systems that are amenable to theoretical studies. Reactions involved in the $Pt^+$-mediated oxidation of methane to methanol (including reactions 1–3) were examined using FTICR experiments by Schwarz and co-workers [6–8]. As part of their detailed experimental and theoretical study [7], they also performed calculations on several reaction pathways, providing geometries and energies for a number of transition states. In one of their earlier Letters [9], calculations on $PtO^+$ at the CAS-SCF level, including spin–orbit and relativistic core effects, predict a $^4\Sigma$ ground state. Spin–orbit interaction of the $^4\Sigma$ ground state with a $^2\Pi$ excited state splits the $^4\Sigma$ state into two components: a $^4\Sigma_{3/2}$ ground state and a $^4\Sigma_{1/2}$ state 400 $cm^{-1}$ higher in energy [9]. The $^4\Sigma_{3/2}$ ground state is calculated to have a harmonic frequency $\omega_e = 675$ $cm^{-1}$ and equilibrium bond distance $r_e = 1.815$ Å. Density functional calculations at the B3LYP level give the $PtO^+$ bond strength as 290 kJ $mol^{-1}$ with the PCI-80 corrected value of 303 kJ $mol^{-1}$ [7]. The theoretical value is slightly lower than the experimental guided ion beam value of Zhang and Armentrout [10], who give the bond energy as $D_0(PtO^+) = 315 \pm 7$ kJ $mol^{-1}$ ($\sim 26\,300 \pm 600$ $cm^{-1}$).

To date, there have been no reported spectroscopic studies on the $PtO^+$ cation. However, this is not the case for the neutral PtO and anionic $PtO^-$ species. Scullman and co-workers [11–14] photographed the gas phase emission spectra of PtO from 11 200 to 26 300 $cm^{-1}$. Initially identified as having a $^1\Sigma$ ground state, subsequent experiments correctly determined it as being $^3\Sigma_{0^+}$ [13]. Additionally, Bernath and co-workers [15] used Fourier transform emission spectroscopy to study the 7100–8015 $cm^{-1}$ region. Stark spectroscopy by Steimle et al. [16] gives the ground state permanent dipole moment of PtO as 2.77 Debye. Matrix isolation techniques have also been applied to PtO. Jansson and Scullman [17] photographed the absorption spectra of PtO in argon, krypton and xenon matrices from $\sim$11 000 to 40 000 $cm^{-1}$. More recently, Andrews and co-workers [18], report bands at 828 and 823 $cm^{-1}$ assigned to the Pt–O stretch of PtO at two different sites in solid Ar. The 828 $cm^{-1}$ band is reported to be in good agreement with B3LYP calculated frequencies for the $^3\Sigma$ ground state of neutral PtO. Lineberger and co-workers [19] obtained the photoelectron spectrum of the $PtO^-$ anion, observing transitions from both the excited $^2\Pi_{1/2}$ and $^2\Pi_{3/2}$ ground state. They observe transitions to the $^3\Sigma_{0^+}$ ground state of neutral PtO as well as to two previously unobserved low-lying $^3\Pi$ states. A spin–orbit splitting of $3580 \pm 40$ $cm^{-1}$ was found between the $^3\Pi_2$ and $^3\Pi_1$ states.

Transition metal-containing diatomics often have predissociative electronic states whose spectra yield a wealth of information. Previous studies in our laboratory on $FeO^+$ and $FeO^+ + CH_4$ intermediates [20,21] as well as $NiS^+$ and $FeS^+$ [22] have shown that detailed vibrational and rotational information along with thermodynamic information can be gained from the analysis of these spectra. We continue our series of studies on the species involved in the conversion of methane to methanol in this Letter with the photofragment spectrum of $PtO^+$.

## 2. Experimental

The experimental apparatus, a dual time-of-flight mass spectrometer, and method have previously been described in detail [20,21] and only specifics to this experiment are given. Platinum cations are generated in a laser-ablation source; however, due to the cost of a solid platinum rod, platinum foil (Sigma–Aldrich, 99.9% pure) was used. For the initial experiments, 0.004″ thick, 1″ square Pt foil was wrapped twice around a threaded rod and secured in place with aluminum endcaps. In later experiments, 0.0025″ thick foil was simply glued to a 0.25″ o.d. aluminum rod whose central portion was machined down to 0.217″ o.d., so that the foil was flush with the outer surface. In both cases, the seam where the foil overlapped led to an unstable ion signal. Once produced, $Pt^+$ ions react with the backing gas mixture which typically

consists of 1–5% $N_2O$ in Ar and He to form $PtO^+$. The plasma undergoes supersonic expansion into vacuum, is skimmed and extracted into the time-of-flight mass spectrometer. $PtO^+$ is isolated by its characteristic flight time and excited at the turning point of the reflectron. Fragment and parent ions are then re-accelerated down the flight tube and detected by a microchannel plate detector. Monitoring the yield of the major $^{195}Pt^+$ isotope from $^{195}Pt^{16}O^+$ (34% natural abundance) as a function of wavelength and normalizing to both parent ion signal and laser fluence produces the photodissociation spectrum. Selected vibrational features of $^{194}Pt^{16}O^+$ and $^{196}Pt^{16}O^+$ were also obtained (33% and 25% natural abundance) to determine isotopic shifts. Unless otherwise indicated, $PtO^+$ refers to the $^{195}Pt^{16}O^+$ isotopomer. Photodissociation of $PtO^+$ was accomplished using both the frequency doubled and mixed output of a pulsed (20 Hz) Nd:YAG-pumped dye laser with a line-width of $<0.2$ cm$^{-1}$ for the frequency-doubled output and slightly narrower for the mixed output, as the YAG is injection seeded.

## 3. Results

Photodissociation of $PtO^+$ in the near-UV region is observed from 25 000 to 30 000 cm$^{-1}$. The entire jet-cooled photofragment spectrum is given in Fig. 1 and shows the complex nature of $PtO^+$. We observe at least 100 vibrational peaks in the 5000 cm$^{-1}$ range covered, which encompass several different electronic states. Many of the vibrational features show partially resolved rotational structure and are usually red-degraded. Towards higher energy, peaks broaden, obscuring rotational structure with background nonresonant dissociation becoming prevalent. This is most likely due to direct dissociation or fast predissociation of some excited states. Individual vibrational peaks are $\sim$10 cm$^{-1}$ wide, reflecting the rotational envelope at the $\sim$10 K beam temperature. A weak, resolved feature observed at 25 317 cm$^{-1}$, whose intensity depends upon source conditions, is identified as a hot band. The onset of nonhot band features is assigned to 25 520 cm$^{-1}$.

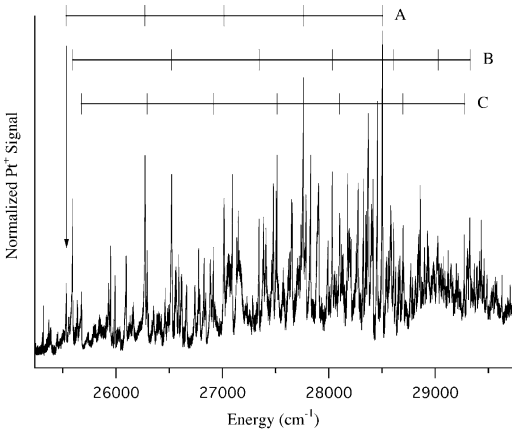


Fig. 1. Photodissociation spectrum of $^{195}Pt^{16}O^+$ from 25 000 to 29 700 cm$^{-1}$. Three excited state vibrational progression are identified (A, B, C) as transitions to $^4\Pi_{-1/2}$, $^4\Pi_{5/2}$ and $^4\Pi_{-1/2}$ states, respectively, from the $^4\Sigma_{3/2}$ ground state. The onset of 25 520 cm$^{-1}$ (indicated by the arrow) gives an upper limit to the $Pt^+$–O bond strength of $D_0(Pt^+–O) \leqslant 305$ kJ mol$^{-1}$. Photodissociation below the arrow is due to a hot band.

## 4. Analysis and discussion

A requirement in photodissociation spectroscopy is that the incident light have sufficient energy to break, in our case, the $Pt^+$–O bond. The spectroscopic onset to photodissociation in the $PtO^+$ spectrum is assigned to 25 520 cm$^{-1}$ (indicated by the arrow in Fig. 1), giving a strict upper limit to the bond strength $D_0(Pt^+–O) \leqslant 305$ kJ mol$^{-1}$. Zhang's [10] value of $D_0(PtO^+) = 315 \pm 7$ kJ mol$^{-1}$, based on guided ion-beam measurements, lies slightly above our spectroscopic threshold. The calculated PCI-80 value of 303 kJ mol$^{-1}$ is in quite good agreement with our value, while the B3LYP value of 290 kJ mol$^{-1}$ is slightly low [7].

A weak, rotationally resolved peak is observed at 25 317 cm$^{-1}$, below our assigned value of $D_0$. The intensity of this peak depends on source conditions, indicating it is a hot band. Rotational structure in the peak was fit to a Hund's case (c) model, with $\Omega$ as the only meaningful quantum number [23]. Fig. 2 shows this band along with the simulated spectrum and the rotational parameters are given within the figure caption. Simulations showed the best fit to have $\Delta\Omega = 0$ and $\Omega = 7/2$. This excludes transitions from a $^4\Sigma_{3/2}$ ground

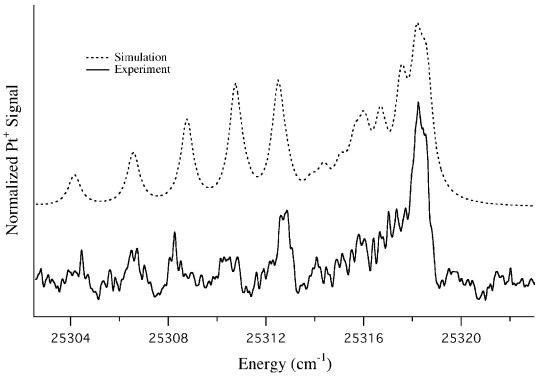


Fig. 2. Hot band observed near 25 318 $cm^{-1}$ (solid line). Rotational simulation (dashed line) assigns the peak as a $\Omega = 7/2 \leftarrow \Omega = 7/2$ transition. Simulation parameters are $\Delta B = B' - B'' = -0.107$ $cm^{-1}$ with $B'' = 0.392$ $cm^{-1}$ and a lifetime of 5 ps.

state, further identifying the peak as a hot band. The most probable transition is from a low-lying, metastable $^4\Delta_7$ state, which Schwarz and coworkers [9] predict to lie 8700 $cm^{-1}$ above the ground state. Rotational analysis shows that the hot band transition involves significant change in the rotational constant $B$. With such an increase in bond length, one would expect a long vibrational progression. We were unable to identify additional vibrational features from this transition, likely due to peak broadening and interference from the much more intense transitions from the ground state.

In order to characterize excited electronic states of $PtO^+$, we tried to identify vibrational progressions in the spectrum. The criteria used for identifying progressions were a fairly long series, a good fit to a Morse progression, reasonable intensities, and a consistent rotational profile. Many of the vibrational peaks in the spectrum could not be assigned to a progression using the outlined criteria. This is most likely due to strong perturbations by nearby states. Only three progressions could be identified with any confidence using the above conditions. All progressions showed an increase in bond length, leading to the observed red tailing. The excited state vibrational progressions, all originating from the $^4\Sigma_{3/2}$ ground state, are identified and vibrational constants for the upper states are given in Table 1. Bond lengths and

Table 1
Vibrational parameters

| Progression | Upper state constants | | | |
|---|---|---|---|---|
| | Peak ($cm^{-1}$) | $\omega_e$ ($cm^{-1}$) | $\omega_e x_e$ ($cm^{-1}$) | $r_e$ (Å) |
| A | 25 530 | 743 | 0 | 1.965 (0.02) |
| B | 25 595 | 1069 | 63.9 | 1.930 (0.02) |
| C | 25 675 | 630 | 4.3 | 1.945 (0.02) |

Ground state parameters were held fixed in all simulations based on the calculated results from [9]: $r''_e = 1.815$ Å and $\omega''_e = 675\,cm^{-1}$. Bond lengths $r_e$ are based on a Franck–Condon fit and error bars are given in parentheses, see text for details.

anharmonicities were obtained from a Franck–Condon analysis using Morse potentials for the ground and excited electronic states. Error bars for $r_e$ (given in parentheses) were estimated by varying the bond length and comparing calculated and experimental intensities. The rotational analysis used to assign the excited states is described in detail below. Isotope shifts were obtained by simultaneously monitoring the yield of the minor $^{194}Pt^+$ and $^{196}Pt^+$ isotopes as a function of the dissociation laser wavelength. Observed shifts confirmed the excited state vibrational numbering in the identified series. Progression A consists of five peaks with a harmonic vibrational spacing of $\omega_e = 743$ $cm^{-1}$. The first peak in this series was used to assign the spectroscopic onset. Rotational analysis shows that the upper state is $^4\Pi_{-1/2}$. Progression C is also to a $^4\Pi_{-1/2}$ excited state. This series consists of seven peaks with a spacing of $\omega_e = 630$ $cm^{-1}$ and a small anharmonicity of $\omega_e x_e = 4.3$ $cm^{-1}$. The final series, Progression B, is to a $^4\Pi_{5/2}$ excited state consisting of seven peaks with $\omega_e = 1070$ $cm^{-1}$ and a large anharmonicity of $\omega_e x_e = 64$ $cm^{-1}$.

As this is the first spectroscopic study of $PtO^+$ we turn to calculations on $PtO^+$ to help us characterize the structure and bonding in this molecule. As a starting point, theory predicts a $^4\Sigma_{3/2}$ ground state with the $^4\Sigma_{1/2}$ state lying 400 $cm^{-1}$ higher. The ground state valence molecular orbital configuration is represented by $2\sigma^2 1\pi^4 1\delta^4 2\pi^2 3\sigma^1$ [9]. Orbitals possessing bonding character are the filled $2\sigma$ (O $2p_z$ with Pt 6s and $5d_{z^2}$) and $1\pi$ (O $2p_x$, $2p_y$

with Pt $5d_{xz}$, $5d_{yz}$) orbitals. The $1\delta$ orbital contains only the Pt $5d_{xy}$ and $5d_{x^2-y^2}$ orbitals and is nonbonding. The $3\sigma$ and the $2\pi$ orbitals are weakly antibonding versions of the $2\sigma$ and $1\pi$ orbitals. Filling these orbitals leads to a weakening of the $Pt^+$–O bond and may account for its catalytic activity.

Various Hund's coupling cases have been used to describe states having a $^4\Sigma$ configuration. It is the interaction with nearby electronic states that gives rise to the splitting between states with $|\Omega| = 1/2$ and $|\Omega| = 3/2$. The use of specific Hund's cases depends on the degree of contamination by other states [24]. With very little admixture of states, the $\Omega$ levels are not split by an amount large compared to $BJ$ and Hund's coupling case ($b$) is most appropriate. A transition to case ($a$) occurs as the amount of contamination increases and the splitting between $\Omega$ levels becomes large compared to $BJ$. However, for a $\Sigma$ state $\Lambda = 0$, and a pure case ($a$) cannot exist. Kopp and Hougen [24] suggest the introduction of an intermediate coupling case for $\Sigma$ states they call ($a'$). The intermediate case follows all the rules for case ($a$) and differs only in the description of how the values of $\Omega$ are split. In states with $\Lambda \neq 0$, the multiplet splitting arises within the specific state and is a first-order phenomenon. When $\Lambda = 0$, the multiplet splitting is a second-order phenomenon due to interactions with nearby states with $\Lambda > 0$. Finally, a transition into case ($c$) occurs when the $\Sigma$ state becomes very strongly perturbed. Again, the rotational spacing has the same form as in case ($a'$); however, the *only* good quantum number is $\Omega$. In each case, states with the same value of $|\Omega|$ are basically degenerate with the splitting between the $|\Omega| = 1/2$ and $|\Omega| = 3/2$ states approximately equal to $4\lambda$. The second-order spin–orbit parameter $\lambda$ also includes the effect of spin–spin interactions, but for diatomics containing a transition metal, second-order spin–orbit effects dominate [25]. The nature of the low-lying states is therefore needed to determine what sort of interactions could occur and to apply the appropriate Hund's coupling case.

Spectroscopic studies on transition metal diatomics with a $^4\Sigma$ ground state provide a yardstick for the possible perturbations in our case. The first-row species CrN [26] and VO [27] have been extensively studied and their $X^4\Sigma$ ground states are accurately known. Very little admixture of states is present in these systems, which have $\lambda = 3$ cm$^{-1}$ and $\lambda = 2$ cm$^{-1}$ for CrN and VO, respectively. Additionally, the second-row diatomics MoN [26] and NbO [28] have well characterized $X^4\Sigma$ ground states. Only slightly more admixture of states is present compared to the first-row species as indicated by $\lambda = 20$ cm$^{-1}$ (MoN) and $\lambda = 16$ cm$^{-1}$ (NbO). It follows that case ($a$) coupling was used to describe the ground states at low values of $J$. The ground state of NbO rapidly uncouples to Hund's case ($b$) with increasing rotation. Experiments on neutral PtO show the splitting between the $^3\Sigma_{0^+}$ ground state and the $^3\Sigma_1$ state to be 930 cm$^{-1}$. Due to the large amount of perturbation, Hund's coupling case ($c$) is used to describe the $^3\Sigma_{0^+}$ ground state [13]. In $PtO^+$ the calculated [9] multiplet splitting is 400 cm$^{-1}$, giving $\lambda = -100$ cm$^{-1}$. This moderate amount of perturbation makes a Hund's case ($a'$) most appropriate. Allowed transitions within case ($a'$) coupling are limited to $^4\Pi_{1/2}$, $^4\Pi_{3/2}$ and $^4\Sigma_{1/2}$ states from the $^4\Sigma_{1/2}$ state and to $^4\Pi_{-1/2}$, $^4\Pi_{5/2}$ and $^4\Sigma_{3/2}$ states from the $^4\Sigma_{3/2}$ ground state.

For the first peak in each of the three identified vibrational progressions, the ground state was fit to the rotational Hamiltonian [25,29,30]

$$H = B''(\boldsymbol{J} - \mathbf{S})^2 + \frac{2}{3}\lambda''(3S_z^2 - \mathbf{S}^2), \tag{4}$$

and the excited $\Pi$ states were fit using

$$H = B'(\boldsymbol{J} - \mathbf{S})^2 + A'\Lambda\Sigma. \tag{5}$$

As described above, the nature of $PtO^+$ is such that the intermediate coupling case ($a'$) is most appropriate. Ground state parameters were fixed as $r_e'' = 1.815$ Å and $\omega_e'' = 675$ cm$^{-1}$ based on the theoretical calculations of Schwarz and co-workers [9]. Additionally, the multiplet splitting in the ground state is calculated as 400 cm$^{-1}$ giving the second-order spin–orbit coupling constant as $\lambda'' = -100$ cm$^{-1}$, which was held fixed in all simulations. The excited $^4\Pi$ states were modeled using Hund's case ($c$) and by fixing the spin–orbit splitting to be 1000 cm$^{-1}$. Varying the spin–orbit splitting from 1000–5000 cm$^{-1}$ had no effect on the

simulated rotational band contour. In all of the rotational simulations, a resolution of 1 $cm^{-1}$ was able to capture all of the observed rotational structure, giving an excited state lifetime of 5 ps, likely due to predissociation. At this modest resolution, it is desirable to constrain the rotational constants as much as possible and the only variable in the simulations was the excited state rotational constant $B'$.

Rotational simulations were performed for both $^4\Pi$–$^4\Sigma$ and $^4\Sigma$–$^4\Sigma$ transitions. Although several peaks in the spectrum are due to $^4\Sigma$–$^4\Sigma$ transitions, they could not be fit to an identifiable vibrational progression and will not be discussed further. Additionally, no transitions were seen from the $^4\Sigma_{1/2}$ state, further confirming the theoretical prediction of a $^4\Sigma_{3/2}$ ground state [9]. Progressions A–C are all due to $^4\Pi$–$^4\Sigma_{3/2}$ transitions.

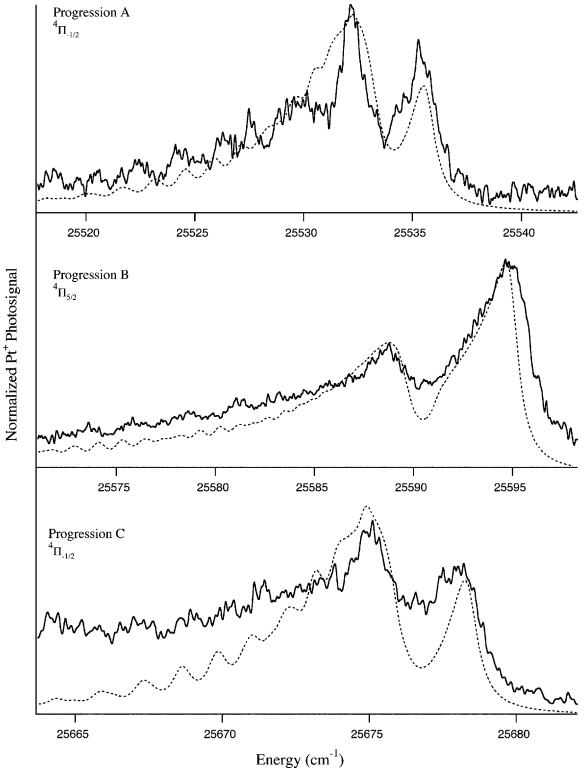


Fig. 3. Rotational simulation (dashed lines) of the first peak for each of the three identified vibrational progressions. A resolution of 1 $cm^{-1}$ was able to capture all of the rotational structure. Parameters used in the rotational simulation are given in Table 2.

Table 2
Rotational simulations

| Upper state constants | Transition | | |
|---|---|---|---|
| | $^4\Pi_{-1/2} \leftarrow {}^4\Sigma_{3/2}$ | $^4\Pi_{5/2} \leftarrow {}^4\Sigma_{3/2}$ | $^4\Pi_{-1/2} \leftarrow {}^4\Sigma_{3/2}$ |
| Progression | A | B | C |
| $B'$ ($cm^{-1}$) | 0.305 | 0.327 | 0.306 |
| $r'_o$ (Å) | (1.935) | (1.868) | (1.930) |
| $T_0$ ($cm^{-1}$) | 25612.5 | 25175.5 | 25555.0 |
| $\tau$ (ps) | 5 | 5 | 5 |

Ground state parameters were held fixed in all simulations based on the calculated results from [9]: $r''_e = 1.815$ Å and $\omega''_e = 675$ $cm^{-1}$. The values of $r'_e$ are given in parentheses, see text for details.

Best-fit simulations are shown along with the experimental data in Fig. 3 and results from rotational analysis of individual peaks are summarized in Table 2. Due to the modest resolution of the spectra, the only free parameter in the simulations is $B'$. This was optimized to reproduce the splitting between and intensity ratio of the peaks for a given transition, as they are the features most sensitive to this parameter. The use of only one adjustable parameter limits our ability to capture the entire peak shape. Because the spin–orbit splitting in the $\Pi$ states is expected to be at least 1000 $cm^{-1}$, the correction to the rotational constant [23], which is approximately $3B/A$, is $<0.1\%$ and is ignored. As mentioned above, progression A is from a $^4\Pi_{-1/2} \leftarrow {}^4\Sigma_{3/2}$ transition. Consistent with the observed red-tailing in the peaks, the bond length increases by 7%. The next progression (B) is due to a $^4\Pi_{5/2} \leftarrow {}^4\Sigma_{3/2}$ transition. Again an increase in bond length of 4% was observed. Similar to peak A, peak C arises from a $^4\Pi_{-1/2} \leftarrow {}^4\Sigma_{3/2}$ transition with a 7% increase in bond length.

## 5. Conclusions

We report the first spectroscopic study of gas phase $PtO^+$. The photodissociation spectrum is very complex due to the high number of excited electronic states. From the observed spectroscopic onset, an upper-limit to the bond strength is given as $D_0(Pt^+–O) \leqslant 305$ kJ $mol^{-1}$. Our spectroscopic value is slightly below the thermodynamic value of

$D_0(PtO^+) = 315 \pm 7$ kJ mol$^{-1}$ determined by Armentrout and co-workers. Vibrational progressions are identified for $^4\Pi_{-1/2} \leftarrow {}^4\Sigma_{3/2}$ and $^4\Pi_{5/2} \leftarrow {}^4\Sigma_{3/2}$ transitions. Rotational analysis of individual peaks within the progressions was used to determine the excited electronic state. A hot band was observed below the spectroscopic onset and identified as a $\Delta\Omega = 0$, $\Omega = 7/2$ transition, most likely a $^4\Delta_{7/2}$ state.

## Acknowledgements

Support for this work by a National Science Foundation Faculty Career Development Award (NSF CHE 9875220) is gratefully acknowledged.

## References

[1] R.H. Crabtree, Chem. Rev. 95 (1995) 987.
[2] J.H. Lunsford, Catal. Today 63 (2000) 165.
[3] H. Schwarz, D. Schröder, Pure Appl. Chem. 72 (2000) 2319.
[4] D. Schröder, H. Schwarz, S. Shaik, Struct. Bond. 97 (2000) 91.
[5] R.B. Metz, in: R.M. Mohan (Ed.), Research Advances in Physical Chemistry, Global, Trivandrum, India, 2001, p. 35.
[6] R. Wesendrup, D. Schröder, H. Schwarz, Angew. Chem. Int. Ed. Engl. 33 (1994) 1174.
[7] M. Pavlov, M.R.A. Blomberg, P.E.M. Siegbahn, R. Wesendrup, C. Heinemann, H. Schwarz, J. Phys. Chem. A 101 (1997) 1567.
[8] C. Heinemann, R. Wesendrup, H. Schwarz, Chem. Phys. Lett. 239 (1995) 75.
[9] C. Heinemann, W. Koch, H. Schwarz, Chem. Phys. Lett. 245 (1995) 509.
[10] X.-G. Zhang, P.B. Armentrout, J. Phys. Chem. A, Submitted, 2003.
[11] C. Nilsson, R. Scullman, N. Mehendale, J. Mol. Spectrosc. 35 (1970) 172.
[12] R. Scullman, U. Sassenberg, C. Nilsson, Can. J. Phys. 53 (1975) 1991.
[13] U. Sassenberg, R. Scullman, J. Mol. Spectrosc. 68 (1977) 331.
[14] U. Sassenberg, R. Scullman, Phys. Scripta 28 (1983) 139.
[15] C.I. Frum, R. Engleman, P.F. Bernath, J. Mol. Spectrosc. 150 (1991) 566.
[16] T.C. Steimle, K.Y. Jung, B.-Z. Li, J. Chem. Phys. 103 (1995) 1767.
[17] K. Jansson, R. Scullman, J. Mol. Spectrosc. 61 (1976) 299.
[18] W.D. Bare, A. Citra, G.V. Chertihin, L. Andrews, J. Phys. Chem. A 103 (1999) 5456.
[19] T.M. Ramond, G.E. Davico, F. Hellberg, F. Svedberg, P. Salen, P. Soderqvist, W.C. Lineberger, J. Mol. Spectrosc. 216 (2002) 1.
[20] J. Husband, F. Aguirre, P. Ferguson, R.B. Metz, J. Chem. Phys. 111 (1999) 1433.
[21] F. Aguirre, J. Husband, C.J. Thompson, K.L. Stringer, R.B. Metz, J. Chem. Phys. 116 (2002) 4071.
[22] J. Husband, F. Aguirre, C.J. Thompson, R.B. Metz, Chem. Phys. Lett. 342 (2001) 75.
[23] G. Herzberg, Molecular Spectra and Molecular Structure. I. Spectra of Diatomic Molecules, Van Nostrand Reinhold Company, New York, 1950.
[24] I. Kopp, J.T. Hougen, Can. J. Phys. 45 (1967) 2581.
[25] H. Lefebvre-Brion, R.W. Field, Perturbations in the Spectra of Diatomic Molecules, Academic Press, London, 1986.
[26] K.C. Namiki, T.C. Steimle, J. Chem. Phys. 111 (1999) 6385.
[27] A.J. Merer, Ann. Rev. Phys. Chem. 40 (1989) 407.
[28] J.L. Femenias, G. Cheval, A.J. Merer, U. Sassenberg, J. Mol. Spectrosc. 124 (1987) 348.
[29] R.M. Gordon, A.J. Merer, Can. J. Phys. 58 (1980) 642.
[30] J.T. Hougen, The Calculation of Rotational Energy Levels and Rotational Line Intensities in Diatomic Molecules, National Bureau of Standards Monograph 115, Washington, DC, 1970.